



UNIVERSITY OF LEEDS

This is a repository copy of *Iron(II) complexes of tridentate indazolyipyridine ligands: enhanced spin-crossover hysteresis and ligand-based fluorescence.*

White Rose Research Online URL for this paper:
<http://eprints.whiterose.ac.uk/83149/>

Version: Accepted Version

Article:

Santoro, A, Kershaw Cook, LJ, Kulmaczewski, R et al. (3 more authors) (2015) Iron(II) complexes of tridentate indazolyipyridine ligands: enhanced spin-crossover hysteresis and ligand-based fluorescence. *Inorganic chemistry*, 54 (2). 682 - 693. ISSN 0020-1669

<https://doi.org/10.1021/ic502726q>

Reuse

Items deposited in White Rose Research Online are protected by copyright, with all rights reserved unless indicated otherwise. They may be downloaded and/or printed for private study, or other acts as permitted by national copyright laws. The publisher or other rights holders may allow further reproduction and re-use of the full text version. This is indicated by the licence information on the White Rose Research Online record for the item.

Takedown

If you consider content in White Rose Research Online to be in breach of UK law, please notify us by emailing eprints@whiterose.ac.uk including the URL of the record and the reason for the withdrawal request.



eprints@whiterose.ac.uk
<https://eprints.whiterose.ac.uk/>

Iron(II) Complexes of Tridentate Indazolyipyridine Ligands. Enhanced Spin-Crossover Hysteresis, and Ligand-Based Fluorescence.

*Amedeo Santoro[†], Laurence J. Kershaw Cook[†], Rafal Kulmaczewski[†], Simon A. Barrett[†],
Oscar Cespedes[§] and Malcolm A. Halcrow^{*†}*

[†]School of Chemistry, University of Leeds, Woodhouse Lane, Leeds LS2 9JT, UK.

[§]School of Physics and Astronomy, University of Leeds, E. C. Stoner Building,
Leeds LS2 9JT, UK.

ABSTRACT

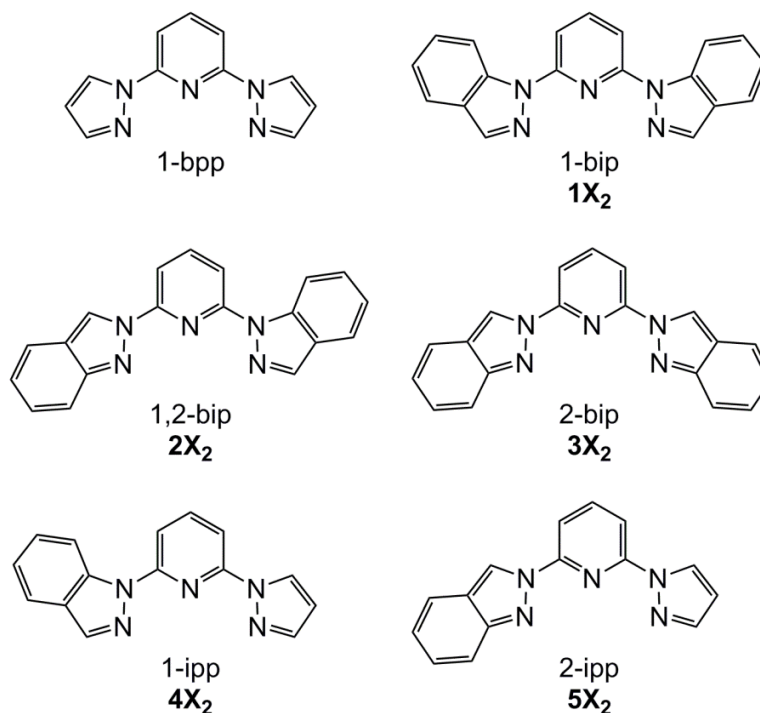
Reaction of 2,6-difluoropyridine with 2 equiv indazole and NaH at room temperature affords a mixture of 2,6-*bis*(indazol-1-yl)pyridine (1-bip), 2-(indazol-1-yl)-6-(indazol-2-yl)pyridine (1,2-bip) and 2,6-*bis*(indazol-2-yl)pyridine (2-bip), which can be separated by solvent extraction. A two-step procedure using the same conditions also affords both 2-(indazol-1-yl)-6-(pyrazol-1-yl)pyridine (1-ipp) and 2-(indazol-1-yl)-6-(pyrazol-2-yl)pyridine (2-ipp). These are all annelated analogues of 2,6-di(pyrazol-1-yl)pyridine, an important ligand for spin-crossover complexes. Iron(II) complexes $[\text{Fe}(1\text{-bip})_2]^{2+}$, $[\text{Fe}(1,2\text{-bip})_2]^{2+}$ and $[\text{Fe}(1\text{-ipp})_2]^{2+}$ are low-spin at room temperature, reflecting a sterically imposed conformational rigidity of the 1-indazolyl ligands. In contrast the 2-indazolyl complexes $[\text{Fe}(2\text{-bip})_2]^{2+}$ and $[\text{Fe}(2\text{-ipp})_2]^{2+}$ are high-spin in solution at room temperature, while salts of $[\text{Fe}(2\text{-bip})_2]^{2+}$ exhibit thermal spin-transitions in the solid state. Notably $[\text{Fe}(2\text{-bip})_2][\text{BF}_4]_2 \cdot 2\text{MeNO}_2$ adopts a terpyridine embrace lattice structure and undergoes a spin-transition near room temperature after annealing, with thermal hysteresis that is wider than previously observed for this structure type ($T_{1/2} = 266 \text{ K}$, $\Delta T = 16\text{-}20 \text{ K}$). That reflects enhanced mechanical coupling between the cations in the lattice through interdigitation of their ligand arms, which supports a previously proposed structure:function relationship for spin-crossover materials with this form of crystal packing. All the compounds in this work exhibit blue fluorescence in solution under ambient conditions. In most cases the ligand-based emission maxima are slightly red shifted upon complexation, but there is no detectable correlation between the emission maximum and the spin state of the iron centers.

Introduction

The use of molecule-based spin-crossover materials¹⁻⁴ as switchable components in macroscopic and nano-scale devices is well-established.⁴⁻⁶ One of the challenges for the development of these applications is the small number of known compounds with technologically favorable switching properties; that is, with spin-transitions centered at room temperature with 30-50 K thermal hysteresis.⁷⁻⁹ The design of new spin-transition materials *de novo* is a challenge of molecular crystal engineering, that still remains to be solved. Progress towards that goal is hindered by the limited number of structure:function correlations that have been established in spin-crossover crystals, which can be generalized to a range of materials.¹⁰

We have previously proposed one such relationship between a spin transition and crystal lattice in a molecular material, in a number of $[\text{Fe}(\text{1-bpp})_2]\text{X}_2$; 1-bpp = 2,6-*bis*{pyrazol-1-yl}pyridine; $\text{X}^- = \text{BF}_4^-, \text{ClO}_4^-$ etc) derivatives.^{11,12} These exhibit spin-transitions that vary in temperature but are very similar in appearance, each taking place abruptly with a small (2-3 K) thermal hysteresis loop.^{12,13} The consistent form of the transitions is retained whether or not the materials undergo a change in crystallographic symmetry during the spin-state change. Although they are not isostructural, the compounds all adopt different forms of the “terpyridine embrace” crystal packing motif, where the (idealized) D_{2d} -symmetric cations associate into layers through interdigitation of their pyrazolyl arms.¹⁴ Neighboring cations within the layers interact strongly, through face-to-face and edge-to-face $\pi \dots \pi$ interactions between their pyrazolyl rings. However, intermolecular interactions between the layers are much weaker van der Waals contacts. This led us to suggest that the consistent spin-crossover cooperativity we observed for this lattice type is transmitted through the material in two dimensions, within the terpyridine embrace layers.

Chart 1 Ligands referred to in this work, and the numbers assigned to their iron(II) complexes in the text ($X^- = \text{BF}_4^-$ or ClO_4^-).



While this proposal is supported by circumstantial evidence,¹¹ the clearest demonstration would be to systematically change the intermolecular interactions inside the layers. That could be achieved with $[\text{Fe}(\text{2-bip})_2]^{2+}$ (2-bip = 2,6-*bis*{indazol-2-yl}pyridine; Chart 1), whose rigid annelated ligands would strengthen the $\pi \dots \pi$ contacts in the terpyridine embrace structure and thus afford increased spin-crossover hysteresis. That goal was hindered by synthetic challenges, since published routes to bip derivatives afford predominantly the alternative isomer 2,6-*bis*{indazol-1-yl}pyridine (1-bip).¹⁵⁻¹⁷ However, we returned to this chemistry following a recent report that the high temperature and extended reaction times that are usually required for bip synthesis^{11,15} can be avoided, by coupling indazolide anions with 2,6-difluoropyridine

precursors.¹⁷ Although this published method still gave a 1-bip derivative as the major product, we reasoned the milder conditions might give higher yields of the thermodynamically disfavored 2-bip isomer.¹⁸ In this way we have now achieved the synthesis of 2-bip, as well as obtaining the unsymmetric derivatives 2-{indazol-1-yl}-6-(pyrazol-1-yl)pyridine (1-ipp) and 2-{indazol-2-yl}-6-(pyrazol-1-yl)pyridine (2-ipp) in useful quantities for the first time.¹⁵ We report here the synthesis of these ligands, and an investigation of their iron(II) complex chemistry.

Experimental

Unless otherwise stated, all reactions were carried out in air using as-supplied AR-grade solvents. All reagents and solvents were purchased commercially and used as supplied.

Syntheses of 2,6-bis-(indazol-1-yl)pyridine (1-bip), 2-(indazol-1-yl)-6-(indazol-2-yl)pyridine (1,2-bip) and 2,6-bis-(indazol-2-yl)pyridine (2-bip). A solution of indazole (2.5 g, 21 mmol) in *N,N*-dimethylformamide (100 cm³) under N₂ was placed at 0 °C in a water-ice bath. Solid NaH (60 wt % in mineral oil; 0.85 g, 21 mmol) was added slowly to the stirred solution and the mixture was stirred for a further 20 mins while keeping the temperature under control. 2,6-difluoropyridine (0.80 g, 7.0 mmol) was then added to the suspension, and the mixture was stirred at room temperature for 2 hrs. Quenching the reaction with water (400 cm³) afforded an off-white precipitate, which was collected by filtration and dried *in vacuo*. The crude product contains 1-bip, 1,2-bip and 2-bip which were separated by repeatedly washing the mixture with diethyl ether at room temperature. The contents of each washing were monitored by thin-layer chromatography; early fractions contain predominantly 1-bip, contaminated with ≤10 % 1,2-bip,

while pure 1,2-bip was obtained in later fractions. The solid residue, when the other components had been removed, contained pure 2-bip. If required, the separated ligands were recrystallized from dichloromethane/pentane. Yields: 1-bip 0.63 g, 29 %; 1,2-bip 0.52 g, 24 %; 2-bip 0.48 g, 22 %. Analytical and spectroscopic data for 1-bip and 1,2-bip were consistent with literature values.^{15,16} Crystal structures confirming the identities of all these isomeric products are presented in the Supporting Information.

For 2-bip: M.p. 279-281 °C. Elemental analysis for C₁₉H₁₃N₅ found, (calcd) (%): C 73.4 (73.3), H 4.20 (4.21), N 22.7 (22.5). ESMS *m/z* 334.1 [Na(2-bip)]⁺, 645.2 [Na(2-bip)₂]⁺. ¹H NMR (CDCl₃) δ 7.15 (pseudo-t, 7.5 Hz, 2H, Ind H⁵), 7.37 (pseudo-t, 7.2 Hz, 2H, Ind H⁶), 7.78 (m, 4H, Ind H⁴ and H⁷), 8.11 (t, 7.9 Hz, 1H, Py H⁴), 8.29 (d, 7.9 Hz, 2H, Py H^{3/5}), 9.19 (s, 1H, Ind H³). ¹³C NMR (CDCl₃) δ 112.6 Py (C^{3/5}), 118.2 (Ind C⁷), 120.6 and 121.1 (Ind C⁴ and C⁵), 122.5 (Ind C^{3a}), 123.2 (Ind C⁶), 128.0 (Ind C³), 141.8 (Py C⁴), 150.5 and 150.6 (Py C^{2/6} and Ind C^{7a}).

Syntheses of 2-fluoro-6-(indazol-1-yl)pyridine and 2-fluoro-6-(indazol-2-yl)pyridine. A 60% NaH dispersion in mineral oil (2.1 g, 51.7 mmol) was stirred in *N,N*-dimethylformamide (70 cm³) under N₂ for 10 mins before 2,6-difluoropyridine (2.7 cm³, 29.8 mmol) was added by syringe. The temperature was lowered to 0°C, and 1*H*-indazole (2.4 g, 20.6 mmol) was added in small portions over a period 1 hr. Once H₂ evolution had ceased, the contents of the vessel were allowed to warm to room temperature and stirred for a further 16 hr. Water was then added dropwise to slowly quench the mixture, which was then diluted to 150 cm³ with additional H₂O. The off-white precipitate was collected and washed with H₂O. After overnight desiccation, the two products were isolated by flash silica column chromatography (CH₂Cl₂ eluent).

For 2-fluoro-6-(indazol-1-yl)pyridine: Rf 0.84. Yellowish oil which solidifies into an off-white crystalline solid upon standing, 2.07 g, 47 % yield. M.p. 77-79 °C. Elemental analysis for C₁₂H₈FN₃ found, (calcd) (%): C 67.9 (67.6), H 3.90 (3.78), N 19.5 (19.7). ESMS *m/z* 214.1 [M+H]⁺. ¹H NMR (CDCl₃) δ 6.76 (dd, 5.4 and 7.7 Hz, 1H, Py H³), 7.31 (pseudo-t, 8.2 Hz, 1H, Ind H⁶), 7.56 (pseudo-t, 7.7 Hz, 1H, Ind H⁵), 7.78 (d, 7.7 Hz, 1H, Ind H⁴), 7.87-7.95 (m, 2H, Py H⁴ and H⁵), 8.21 (s, 1H, Ind H³), 8.83 (d, 9.0 Hz, 1H, Ind H⁷). ¹³C NMR (CDCl₃) δ 104.0 (d, 144.3 Hz, Py C³), 109.6 (d, 16.5 Hz, Py C⁵), 115.4 (Ind C⁷), 120.8 (Ind C⁴), 122.9 (Ind C⁵), 126.1 (Ind C^{3a}), 128.3 (Ind C⁶), 137.6 (Ind C³), 138.8 (Ind C^{7a}), 142.7 (d, 33.0 Hz, Py C⁴), 152.5 (d, 61.9 Hz, Py C⁶), 162.1 (d, 952.5 Hz, Py C²). ¹⁹F NMR (CDCl₃) δ -68.6 (d, 5.4 Hz).

For 2-fluoro-6-(indazol-2-yl)pyridine: Rf: 0.59. White solid, 0.72 g, 16 % yield. M.p. 148-150 °C. Elemental analysis for C₁₂H₈FN₃ found, (calcd) (%): C 67.3 (67.6), H 3.80 (3.78), N 19.6 (19.7). ESMS *m/z* 214.1 [M+H]⁺, 237.1 [M+Na]⁺. ¹H NMR (CDCl₃) δ 6.94 (pseudo-t, 7.9 Hz, 1H, Py H³), 7.11 (dd, 6.4 and 8.7 Hz, 1H, Ind H⁵), 7.34 (dd, 6.4 and 9.1 Hz, 1H, Ind H⁶), 7.72 (pseudo-t, 8.7 Hz) and 7.74 (pseudo-t, 9.1 Hz; both 1H, Ind H⁴ and H⁷), 8.00 (pseudo-t, 7.9 Hz, 1H, Py H⁴), 8.18 (dd, 1.9 and 7.9 Hz, 1H, Py H⁵), 9.03 (s, 1H, Ind H³). ¹³C NMR (CDCl₃) δ 107.7 (d, 140.2 Hz, Py C³), 110.7 (d, 20.7 Hz, Py C⁵), 118.0 (Ind C⁷), 121.0 and 121.2 (Ind C⁴ and C⁵), 122.5 (Ind C^{3a}), 123.0 (Ind C⁶), 128.0 (Ind C³), 143.5 (d, 33.0 Hz, Py C⁴), 150.2 (d, 49.5 Hz, Py C⁶), 150.6 (Ind C^{7a}), 162.2 (d, 964.9 Hz, Py C²). ¹⁹F NMR (CDCl₃) δ -67.6 (d, 7.6 Hz).

Synthesis of 2-(indazol-1-yl)-6-(pyrazol-2-yl)pyridine (1-ipp). A 60% mineral oil dispersion of NaH (0.70 g, 17.5 mmol) was suspended in *N,N*-dimethylformamide (50 cm³) under an N₂ atmosphere. 1*H*-pyrazole (0.47 g, 6.83 mmol) was added to the stirring suspension gradually. After the gas evolution subsided, 2-fluoro-6-(indazol-1-yl)pyridine (1.17 g, 5.47 mmol) was

added and the mixture was stirred for 5 hrs. The reaction was quenched carefully with water, then diluted further to 200 cm³ volume to afford an off-white precipitate that was collected by filtration and washed with water. The dried solid was purified by trituration with hexane (40 cm³), affording pure 1-ipp as the insoluble residue. White solid, 0.75 g, 52 % yield. M.p. 109-111 °C. Elemental analysis for C₁₅H₁₁N₅ found, (calcd) (%): C, 68.6 (68.9), H 4.35 (4.42), N 26.5 (26.8). The NMR and mass spectra for this compound were consistent with the literature data.¹⁵

Synthesis of 2-(indazol-1-yl)-6-(pyrazol-2-yl)pyridine (2-ipp). Method as for 1-ipp, using 2-fluoro-6-(indazol-1-yl)pyridine (1.17 g, 5.47 mmol) as reagent. Colorless powder, 1.17 g, 82 % yield. M.p. 118-120 °C. Elemental analysis for C₁₅H₁₁N₅ found, (calcd) (%): C, 68.7 (68.9), H 4.20 (4.42), N 27.0 (26.8). ESMS *m/z* 284.1 [H(2-bip)]⁺, 284.1 [Na(2-bip)]⁺. ¹H NMR (CDCl₃) δ 6.55 (dd, 1.7 and 2.6 Hz, 1H, Pz *H*⁴), 7.13 (dd, 6.9 and 8.6 Hz, 1H, Ind *H*⁵), 7.35 (dd, 6.7 and 8.8 Hz, 1H, Ind *H*⁶), 7.73-7.79 (m, 2H, Ind *H*⁴ and *H*⁷), 7.80 (d, 1.7 Hz, 1H, Pz *H*³), 7.99 (d, 8.1 Hz, 1H, Py *H*⁵), 8.03 (pseudo-t, 7.7 Hz, 1H, Py *H*⁴), 8.17 (d, 7.5 Hz, 1H, Py *H*³), 8.66 (d, 2.6 Hz, 1H, Pz *H*⁵), 9.11 (s, 1H, Ind *H*³). ¹³C NMR (CDCl₃) δ 108.2 (Pz *C*⁴), 111.0 and 111.1 (Py *C*³ and *C*⁵), 118.1 (Ind *C*⁷), 120.5 and 121.1 (Ind *C*⁴ and *C*⁵), 122.4 (Ind *C*^{3a}), 123.0 (Ind *C*⁶), 127.1 (Pz *C*⁵), 127.8 (Ind *C*³), 141.6 (Py *C*⁴), 142.6 (Pz *C*³), 150.3 (2C, Py *C*² and Py *C*⁶), 150.5 (Ind *C*^{7a}).

Syntheses of [Fe(1-bip)₂][ClO₄]₂ (1[ClO₄]₂) and [Fe(1,2-bip)₂][ClO₄]₂ (2[ClO₄]₂). These salts were prepared by stirring Fe[ClO₄]₂·6H₂O (0.17 g, 0.48 mmol) with the appropriate ligand 1-bip or 1,2-bip (0.30 g, 0.96 mmol) in nitromethane (25 cm³) at room temperature, until all the solid had dissolved. The solutions were filtered and concentrated, and then excess diethyl ether

was added to precipitate the products as dark brown microcrystals. Both compounds adopt monohydrate formulations after air drying by microanalysis. Elemental analysis for $1[\text{ClO}_4]_2 \cdot \text{H}_2\text{O}$, $\text{C}_{38}\text{H}_{26}\text{B}_2\text{F}_8\text{FeN}_{10} \cdot \text{H}_2\text{O}$ found, (calcd) (%): C 50.6 (51.0), H 3.00 (3.15), N 15.7 (15.6). Elemental analysis for $2[\text{ClO}_4]_2 \cdot \text{H}_2\text{O}$, $\text{C}_{38}\text{H}_{26}\text{B}_2\text{F}_8\text{FeN}_{10} \cdot \text{H}_2\text{O}$ found, (calcd) (%): C 50.6 (51.0), H 3.10 (3.15), N 15.8 (15.6).

Synthesis of $[\text{Fe}(2\text{-bip})_2][\text{BF}_4]_2$ ($3[\text{BF}_4]_2$). A mixture of 2-bip (0.30 g, 0.96 mmol) and $\text{Fe}[\text{BF}_4]_2 \cdot 6\text{H}_2\text{O}$ (0.16 g, 0.48 mmol) in acetonitrile (15 cm^3) was stirred at room temperature for 16 hrs. The solution was filtered and concentrated, and the product crystallized by addition of excess diethyl ether. Recrystallisation by slow diffusion of diethyl ether vapor into a nitromethane solution of the complex yielded diffraction quality single crystals, which decomposed from solvent loss on drying *in vacuo*. Yield 0.26 g, 64 %. Elemental analysis for $\text{C}_{38}\text{H}_{26}\text{B}_2\text{F}_8\text{FeN}_{10}$ found, (calcd) (%): C 53.4 (53.6), H 3.00 (3.08), N 16.5 (16.4).

More rapid crystallisation of the compound from this, or other, solvent mixtures instead afforded a feathery amorphous brown material, which contained lattice water by microanalysis. Elemental analysis for $\text{C}_{38}\text{H}_{26}\text{B}_2\text{F}_8\text{FeN}_{10} \cdot 2.5\text{H}_2\text{O}$ found, (calcd) (%): C 50.9 (50.9), H 3.30 (3.48), N 15.9 (15.6).

Alternatively, a solution of $\text{Fe}[\text{BF}_4]_2 \cdot 6\text{H}_2\text{O}$ (0.16 g, 0.48 mmol) in acetone (15 cm^3) was carefully layered onto a solution of 2-bip (0.30 g, 0.96 mmol) in chloroform (25 cm^3). This yielded the complex as polycrystalline material, analysing approximately as $3[\text{BF}_4]_2 \cdot 2.8\text{CHCl}_3$. Elemental analysis for $\text{C}_{38}\text{H}_{26}\text{B}_2\text{F}_8\text{FeN}_{10} \cdot 2.8\text{CHCl}_3$ found, (calcd) (%): C 41.0 (41.3), H 2.90 (2.44), N 12.2 (11.8).

Synthesis of [Fe(2-bip)₂][ClO₄]₂ (3[ClO₄]₂). Method as for 3[BF₄]₂, using Fe[ClO₄]₂·6H₂O (0.17 g, 0.48 mmol). The product was always obtained as a feathery brown amorphous material from nitromethane/diethyl ether, although on one occasion a small number of (twinned) crystals were also present in the sample. Yield 0.25 g, 59 %. Elemental analysis for C₃₈H₂₆Cl₂FeN₁₀O₈·2.5H₂O found, (calcd) (%): C 49.3 (49.5), H 3.00 (3.39), N 15.0 (15.2).

Alternatively, a solution of Fe[ClO₄]₂·6H₂O (0.16 g, 0.48 mmol) in acetone (15 cm³) was carefully layered onto a solution of 2-bip (0.30 g, 0.96 mmol) in chloroform (25 cm³). Single crystals of the chloroform solvate of 3[ClO₄]₂ grew at the interface over a period of days. Elemental analysis for C₃₈H₂₆Cl₂FeN₁₀O₈·CHCl₃ found, (calcd) (%): C 46.6 (47.0), H 2.80 (2.73), N 13.6 (14.0).

Syntheses of [Fe(1-ipp)₂][BF₄]₂ (4[BF₄]₂) and [Fe(1-ipp)₂][ClO₄]₂ (4[ClO₄]₂). A solution of 1-ipp (0.31 g, 1.2 mmol) and either Fe[BF₄]₂·6H₂O (0.20 g, 0.6 mmol) or Fe[ClO₄]₂·6H₂O (0.22 g, 0.6 mmol) in MeNO₂ (30 cm³) was stirred at room temperature for 1 hr. The solution was filtered, and the product was then precipitated by slow addition of diethyl ether (80 cm³). The precipitate was collected and washed with further Et₂O. Golden brown microcrystalline solids, 0.22 g, 45 % yield (4[BF₄]₂) and 0.11 g, 21 % yield (4[ClO₄]₂). Slow diffusion of diethyl ether vapor into nitromethane solutions of the crude compounds yielded the single crystals used for the crystallographic analyses. Both compounds contained nitromethane of crystallization by X-ray crystallography and elemental analysis. Elemental analysis for 4[BF₄]₂·CH₃NO₂, C₃₀H₂₂B₂F₈FeN₁₀·CH₃NO₂ found, (calcd) (%): C 45.7 (45.8), H 2.90 (3.10), N 18.5 (18.9). Elemental analysis for 4[ClO]₂·CH₃NO₂, C₃₀H₂₂Cl₂FeN₁₀O₈·CH₃NO₂ found, (calcd) (%): C 44.3 (44.4), H 2.90 (3.01), N 18.6 (18.4).

Syntheses of [Fe(2-ipp)₂][BF₄]₂ (5**[BF₄]₂) and [Fe(2-ipp)₂][ClO₄]₂ (**5**[ClO₄]₂).** A solution of 2-ipp (0.13 g, 0.48 mmol) and either Fe[BF₄]₂·6H₂O (81 mg, 0.24 mmol) or Fe[ClO₄]₂·6H₂O (87 mg, 0.24 mmol) was stirred in MeNO₂ for 1 hr, then filtered as before. Attempts to isolate these complexes by addition of diethyl ether, or another antisolvent, did not yield solid precipitates. Hence, the compounds were simply isolated by evaporating the solutions to dryness, which afforded solid residues that were washed with Et₂O and dried *in vacuo*. Red powders, 0.16 g, 90 % yield (**5**[BF₄]₂) and 0.13 g, 69 % yield (**5**[ClO₄]₂). Elemental analysis for **5**[BF₄]₂·½H₂O, C₃₀H₂₂B₂F₈FeN₁₀·½H₂O found, (calcd) (%): C 47.7 (47.4), H 3.30 (3.05), N 18.1 (18.4). Elemental analysis for **5**[ClO]₂, C₃₀H₂₂Cl₂FeN₁₀O₈ found, (calcd) (%): C 46.3 (46.4), H 2.90 (2.85), N 18.2 (18.0).

Single crystal X-ray structure determinations

Diffraction data were collected with an Agilent Supernova dual-source diffractometer using monochromated Mo-*K*_α radiation ($\lambda = 0.71073 \text{ \AA}$; **3**[BF₄]₂·2MeNO₂ and **3**[BF₄]₂·*y*CHCl₃) or Cu-*K*_α radiation ($\lambda = 1.51841 \text{ \AA}$; **3**[ClO₄]₂·CHCl₃, **4**[BF₄]₂·MeNO₂, **4**[ClO₄]₂·MeNO₂ and all the organic compounds). Experimental details of structure determinations of the complexes are given in Table 1, while data for the uncomplexed ligand structures are in the Supporting Information. All the structures were solved by direct methods (*SHELXS97*¹⁹), and developed by full least-squares refinement on *F*² (*SHELXL97*¹⁹). Crystallographic figures were prepared using *X-SEED*.²⁰ Unless otherwise stated, all non-H atoms in the structures were refined anisotropically, and C-bound H atoms were placed in calculated positions and refined using a riding model.

Table 1 Experimental details for the crystal structure determinations of the complexes in this study. Crystallographic data for the organic ligand crystal structures are given in the Supporting Information.

	3[BF₄]₂·2MeNO₂		3[BF₄]₂·yCHCl₃		3[ClO₄]₂·CHCl₃		4[BF₄]₂·MeNO₂	4[ClO₄]₂·MeNO₂
formula	C ₄₀ H ₃₂ B ₂ F ₈ FeN ₁₂ O ₄	C ₄₀ H ₃₂ B ₂ F ₈ FeN ₁₂ O ₄	C ₃₉ H ₂₇ B ₂ Cl ₃ F ₈ FeN ₁₀	C ₃₉ H ₂₇ Cl ₃ FeN ₁₀ O ₈	C ₃₉ H ₂₇ Cl ₃ FeN ₁₀ O ₈	C ₃₁ H ₂₅ B ₂ F ₈ FeN ₁₁ O ₂	C ₃₁ H ₂₅ Cl ₂ Fe N ₁₁ O ₁₀	
fw	974.25	974.25	971.53	996.81	996.81	813.09	838.37	
cryst syst	monoclinic	monoclinic	monoclinic	Triclinic	triclinic	monoclinic	monoclinic	
Space group	<i>P</i> 2 ₁ / <i>n</i>	<i>P</i> 2 ₁ / <i>n</i>	<i>C</i> 2/ <i>c</i>	<i>P</i> $\bar{1}$	<i>P</i> $\bar{1}$	<i>P</i> 2 ₁ / <i>c</i>	<i>P</i> 2 ₁ / <i>c</i>	
<i>a</i> /Å	14.0107(5)	14.1074(5)	26.721(5)	12.7312(7)	12.7650(5)	15.0240(2)	15.1486(2)	
<i>b</i> /Å	20.1972(6)	20.3712(7)	25.458(5)	13.2422(8)	13.0619(5)	12.6714(2)	12.7908(2)	
<i>c</i> /Å	14.1012(4)	14.1541(4)	18.792(4)	13.5769(7)	14.2126(6)	17.1017(3)	17.0900(2)	
<i>α</i> /deg	–	–	–	87.610(5)	88.085(3)	–	–	
<i>β</i> /deg	90.854(3)	90.784(3)	110.66(3)	66.525(5)	65.731(4)	91.5520(10)	92.2920(10)	
<i>γ</i> /deg	–	–	–	78.669(5)	81.623(3)	–	–	
<i>V</i> /Å ³	3989.9(2)	4067.3(2)	11961(4)	2056.8(2)	2136.35(15)	3254.54(9)	3308.76(8)	
<i>Z</i>	4	4	12	2	2	4	4	
<i>T</i> /K	100(2)	200(2)	120(2)	120(2)	340(2)	120(2)	120(2)	
<i>D</i> _{calcd} /gcm ⁻³	1.622	1.591	1.619	1.609	1.550	1.659	1.683	
reflns collected	19050	8955	25606	15691	16525	18075	14265	
unique reflns	9500	4484	11423	7682	7958	6417	6426	
<i>R</i> _{int}	0.041	0.024	0.045	0.062	0.036	0.047	0.045	
<i>R</i> ₁ , <i>I</i> > 2σ(<i>I</i>) ^a	0.056	0.070	0.090	0.079	0.085	0.052	0.041	
<i>wR</i> ₂ , all data ^b	0.131	0.176	0.274	0.253	0.286	0.144	0.109	
GoF	1.012	1.028	1.052	1.043	1.034	1.024	1.038	

$$^a R = \sum [|F_o| - |F_c|] / \sum |F_o| \quad ^b wR = [\sum w(F_o^2 - F_c^2) / \sum wF_o^4]^{1/2}$$

The crystal of $3[\text{BF}_4]_2 \cdot 2\text{MeNO}_2$ diffracted substantially less well at 200 K than at 100 K, and observed reflections were only obtained to $2\theta = 42^\circ$ in the higher temperature dataset. That accounts for the lower precision in the bond lengths and angles at this temperature. Further warming led to a strong increase in crystal mosaicity, possibly reflecting solvent loss which was rapid under ambient conditions. No disorder was present in the model at either temperature, and no restraints were applied.

The asymmetric unit of $3[\text{BF}_4]_2 \cdot y\text{CHCl}_3$ ($y \approx 1$) contains 1.5 formula units. That is, one complex cation on general crystallographic site; one half complex cation, whose Fe atom lies on the C_2 axis $\frac{1}{2}, y, \frac{1}{4}$; two whole BF_4^- ions, one of which is disordered; one C_2 -symmetric half anion; and, one disordered, half-occupied anion that spans a crystallographic inversion center. Refined restraints were applied to the B–F and F...F distances in the disordered anion sites. Chloroform was also clearly present in the Fourier map, which was however poorly defined and badly disordered. This was therefore treated using a *SQUEEZE* analysis,²¹ which revealed 557 unresolved electrons per asymmetric unit. That corresponds to 46.5 electrons per formula unit, or 0.8 equiv chloroform (58 electrons per molecule). That solvent content is consistent with a TGA analysis of this material, shown in the Supporting Information (Fig. S18). The *SQUEEZED* dataset was used for the final least squares cycles. All crystallographically ordered non-H atoms were refined anisotropically.

Two datasets were collected from the same crystal of $3[\text{ClO}_4]_2 \cdot \text{CHCl}_3$. Following an initial refinement at 120 K, large and elongated displacement ellipsoids on one of the 2-bip ligands indicated the presence of disorder. This was modelled without restraints, using two orientations for the atoms N(26)-C(40). The relative occupancies of the two ligand orientations refined to 0.53:0.47, so they were both given the occupancy 0.50 in the final refinement. This ligand

disorder was not present in the high temperature structure. Both ClO_4^- ions are also disordered at each temperature, which were modelled using the refined Cl–O and O...O distance restraints. The chloroform solvent site was fully occupied at 120 K but only *ca.* half-occupied at 340 K, implying slow loss of solvent from the crystal during the data collection. All fully occupied non-H atoms, plus the disordered anions in the low temperature structure, were refined anisotropically.

No disorder is present in the refinements of $4[\text{BF}_4]_2 \cdot \text{MeNO}_2$ or $4[\text{ClO}_4]_2 \cdot \text{MeNO}_2$, and no restraints were applied to either model.

Other measurements

Elemental microanalyses were performed by the University of Leeds School of Chemistry microanalytical service. Electrospray mass spectra (ESMS) were obtained on a Bruker MicroTOF spectrometer, from MeCN feed solutions. All mass peaks have the correct isotopic distributions for the proposed assignments. NMR spectra were obtained using a Bruker Avance 500 FT spectrometer, operating at 500.1 MHz (^1H) or 125 MHz (^{13}C). Thermogravimetric analyses employed a TA Instruments TGA 2050 analyser, while the differential scanning calorimetry measurement used a TA Instruments DSC Q20 calorimeter, heating at a rate of 10 K min^{-1} . X-ray powder diffraction measurements were obtained from a Bruker D2 Phaser diffractometer, using Cu- K_α radiation ($\lambda = 1.5419 \text{ \AA}$).

Magnetic susceptibility measurements were performed on a Quantum Design VSM SQUID magnetometer, in an applied field of 5000 G and a temperature ramp of 5 K min^{-1} . Diamagnetic corrections for the samples were estimated from Pascal's constants;²² a previously measured diamagnetic correction for the sample holder was also applied to the data. Magnetic

susceptibility measurements in solution were obtained by Evans method using a Bruker Avance500 spectrometer operating at 500.13 MHz.²³ Tetramethylsilane was added to all the solutions as an internal standard. A diamagnetic correction for the sample,²² and a correction for the variation of the density of the solvent with temperature,²⁴ were applied to these data.

UV/vis spectra were measured using a Perkin Elmer Lambda900 spectrophotometer. Fluorescence measurements under ambient conditions were obtained using a Horiba Fluoromax 3 fluorimeter, with constant slit widths of 2 nm. A range of excitation wavelengths was sampled, and the data quoted are for the excitation wavelength that led to the most intense emission for each compound. The sample concentrations for the fluorescence spectra were $2.8 \times 10^{-5} \text{ mol dm}^{-3}$ (ligands) and $1.0 \times 10^{-6} \text{ mol dm}^{-3}$ (complexes).

Results

Reaction of 2,6-difluoropyridine with 2 equiv indazole in the presence of NaH, in dmf at 298 K, affords a mixture of 1-bip,^{15,16} 1,2-bip¹⁵ and 2-bip after the usual work-up. Separation of these isomers by column chromatography is challenging, but they can be purified by exploiting their solubility in diethyl ether, which follows the order 1-bip > 1,2-bip > 2-bip. Samples of 1-bip obtained in this way usually contain <10 % residual 1,2-bip by NMR, which required multiple recrystallizations to remove, but the other two isomers are obtained in pure form. The three purified ligands were obtained in similar yields, of 22-29 %. Treatment of 2,6-difluoropyridine with just 1 equiv indazole and NaH, in dmf at 298 K as before, affords a mixture containing 2-fluoro-6-(indazol-1-yl)pyridine and 2-fluoro-6-(indazol-2-yl)pyridine which were separated chromatographically. Treatment of each of these intermediates with 1 equiv pyrazole under the

same conditions then gives the unsymmetric ligands 1-ipp or 2-ipp in moderate yields, without the need for an extended purification. While 1-ipp has been reported before,¹⁵ its published synthesis required forcing conditions which led to scrambling of the indazolyl and pyrazolyl substituents during the reaction. That complication was not observed under the milder conditions used in this study. The different bip and ipp ligand isomers can be distinguished by ¹H NMR, with the indazole *H3* resonance appearing at 8.3 ppm for the indazol-1-yl rings in the products, and at 9.1-9.2 ppm for the indazol-2-yl substituents.¹⁵ The identities of all three isomers of bip, plus 2-ipp and the intermediate 2-fluoro-6-(indazol-2-yl)pyridine, were also confirmed crystallographically. The latter compound was obtained in three different polymorphs, exhibiting identical molecular conformations but different modes of crystal packing (Fig. S4, Supporting Information).

The complexes [Fe(1-bip)₂][BF₄]₂ (**1**[BF₄]₂) and [Fe(1,2-bip)₂][BF₄]₂ (**2**[BF₄]₂; Chart 1) have been previously described¹⁵ and are low-spin in the solid state at room temperature.²⁵ The perchlorate salts [Fe(1-bip)₂][ClO₄]₂ (**1**[ClO₄]₂) and [Fe(1,2-bip)₂][ClO₄]₂ (**2**[ClO₄]₂) were prepared in this work, and used for the solution studies described below. Treatment of hydrated Fe[BF₄]₂ or Fe[ClO₄]₂ with 2 equiv 2-bip, 1-ipp or 2-ipp in MeNO₂ yields, after the usual work-up, the new complexes [Fe(2-bip)₂]₂X₂ (X⁻ = BF₄⁻, **3**[BF₄]₂; X⁻ = ClO₄⁻, **3**[ClO₄]₂), [Fe(1-ipp)₂]₂X₂ (X⁻ = BF₄⁻, **4**[BF₄]₂; X⁻ = ClO₄⁻, **4**[ClO₄]₂) and [Fe(2-bip)₂][BF₄]₂ (X⁻ = BF₄⁻, **5**[BF₄]₂; X⁻ = ClO₄⁻, **5**[ClO₄]₂; Chart 1).

Slow diffusion of diethyl ether into a nitromethane solution of **3**[BF₄]₂ yields orange block crystals of formula [Fe(2-bip)₂][BF₄]₂·2MeNO₂ (**3**[BF₄]₂·2MeNO₂). These crystals contain the expected six-coordinate dication, which is low-spin at 100 K according to its metric parameters (Fig. 1 and Table 2). The diffraction quality of the crystals reduced significantly at higher

temperatures, but a less precise refinement at 200 K also demonstrated a low-spin iron centre. The crystals adopt a version of the terpyridine embrace structure in the space group $P2_1/n$, with the interdigitated cation layers parallel to the crystallographic (010) plane (Fig. 2). The terpy embrace layers in $3[\text{BF}_4]_2 \cdot 2\text{MeNO}_2$ are heterochiral, with nearest neighbor cations in the layers being related by the crystallographic n glide plane. It is more common for all molecules in a layer to have the same handedness (although adjacent layers can have the same or opposite handedness in different versions of the structure).¹⁴ In other respects, however, $3[\text{BF}_4]_2 \cdot 2\text{MeNO}_2$ is a typical terpyridine embrace crystal. The interdigitated cations interact with each other through face-to-face $\pi \dots \pi$ interactions (interplanar spacing 3.4 Å at 100 K) and edge-to-face C–H... π contacts (C... π distances 3.7–3.8 Å).

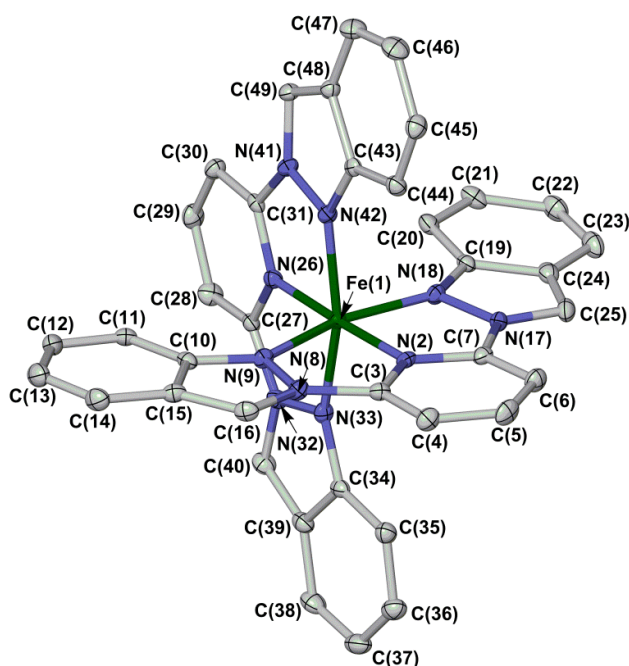


Figure 1. View of the $[\text{Fe}(2\text{-bip})_2]^{2+}$ dication in the structure of $3[\text{BF}_4]_2 \cdot 2\text{MeNO}_2$ at 100 K. Displacement ellipsoids are drawn at the 50 % probability level, and H atoms have been omitted. Color code: C, white; N, blue; Fe, green.

Table 2 Selected bond lengths and angular parameters in the crystal structures of the complexes in this work (Å, deg). The same atom numbering scheme was used for all the solvate structures of **3[BF₄]₂** and **3[ClO₄]₂** (Fig. 1). α , Σ and Θ are indices showing the spin state of the complex,²⁶ while θ and ϕ are measures of the angular Jahn-Teller distortion sometimes shown by these iron centers in their high-spin state.^{11,27,28} Full definitions of these parameters are in the Supporting Information (page S4), and their typical values in high- and low-spin [Fe(bpp)₂]²⁺ derivatives are given in ref. 11.

	3[BF₄]₂·2MeNO₂		3[BF₄]₂·yCHCl₃ Molecule A Half-molecule B		3[ClO₄]₂·CHCl₃	
<i>T</i> / K	100	200	120		120 ^a	340
Fe(1)–N(2)	1.886(2)	1.886(5)	2.125(5)	1.903(4)	2.016(4)	2.138(4)
Fe(1)–N(9)	1.962(2)	1.964(5)	2.161(4)	1.997(4)	2.084(5)	2.192(4)
Fe(1)–N(18)	1.974(2)	1.977(5)	2.203(4)	1.985(4)	2.063(4)	2.177(4)
Fe(1)–N(26)	1.884(2)	1.889(5)	2.111(4)	–	1.868(13)/2.188(15)	2.138(5)
Fe(1)–N(33)	1.966(2)	1.973(5)	2.176(4)	–	1.914(9)/2.257(11)	2.171(5)
Fe(1)–N(42)	1.968(2)	1.965(5)	2.150(4)	–	2.070(4)	2.161(4)
α	80.6(2)	80.5(4)	73.3(3)	79.7(2)	78.2(7)/75.2(7)	73.44(4)
Σ	81.6(3)	82.2(7)	152.8(5)	94.1(5)	105(1)/135(1)	151.3(6)
Θ	269	271	475	294	337/418	467
ϕ	177.08(10)	177.0(2)	168.83(15)	176.7(2)	171.0(4)/170.6(4)	171.14(17)
θ	89.21(1)	89.28(3)	89.69(4)	84.58(4)	89.10(6)/89.60(7)	88.10(5)

^aParameters from both the ligand disorder sites at this temperature are given.

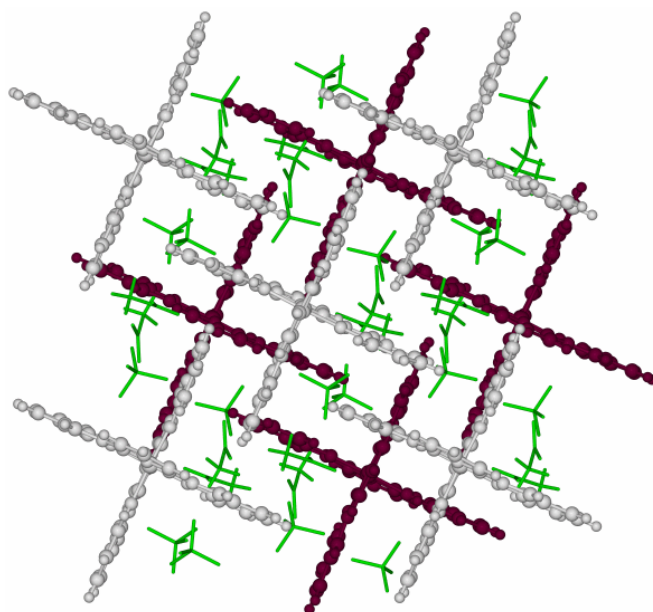


Figure 2. Packing diagram of $3[\text{BF}_4]_2 \cdot 2\text{MeNO}_2$ at 100 K. Alternate layers of $\pi \dots \pi$ stacked cations have pale and dark coloration, and the anions and solvent are de-emphasized for clarity. The view is parallel to the $[010]$ vector with c vertical.

Magnetic susceptibility measurements on freshly prepared, crystalline $3[\text{BF}_4]_2 \cdot 2\text{MeNO}_2$ confirmed its low-spin nature at room temperature. However, $\chi_M T$ increased rapidly from 0.2 to $3.1 \text{ cm}^3 \text{ mol}^{-1} \text{ K}$ upon heating to 350 K, indicating conversion to a high-spin state (Fig. 3). Microanalysis and TGA showed this spin- conversion is accompanied by loss of nitromethane, yielding solvent-free $3[\text{BF}_4]_2$. The dried material undergoes an abrupt, complete thermal spin transition just below room temperature with a 20 K hysteresis loop on the first scan ($T_{1/2\downarrow} = 260$ and $T_{1/2\uparrow} = 280$ K). On repeated scanning the transition becomes sharper, and the hysteresis narrows slightly to 16 K ($T_{1/2\downarrow} = 258$ and $T_{1/2\uparrow} = 274$ K). Such behavior has been observed before

for hysteretic spin-transitions, as the structural changes associated with the transition are annealed into the material upon repeated cycling.^{29,30} DSC measurements showed an endotherm and exotherm at slightly lower temperatures than the magnetic data ($T_{1/2\downarrow} = 254.3$, $T_{1/2\uparrow} = 267.1$ K; $\Delta H = 15.5$ kJmol⁻¹, $\Delta S = 59$ Jmol⁻¹K⁻¹). These thermodynamic parameters are typical for first order spin-transitions.³¹ Notably, although its hysteresis is wider, the overall midpoint temperature of this transition ($T_{1/2} = 266$ K, $\Delta T = 16$ -20 K) is very similar to the parent complex [Fe(1-bpp)₂][BF₄]₂ ($T_{1/2} = 260$ K, $\Delta T = 3$ K).¹²

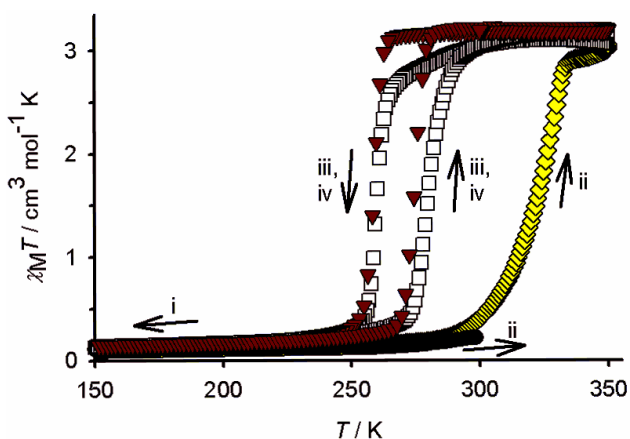


Figure 3. Magnetic susceptibility data for **3[BF₄]₂**. The sample was: (i) cooled from 295 → 3 K (black circle); (ii) warmed from 3 → 350 K (yellow diamond); (iii) and (iv) cycled twice between 350 → 3 → 350 K (white squares, red triangles).

X-ray powder diffraction on **3[BF₄]₂·2MeNO₂**, that had been exposed to air, showed it to be poorly crystalline at 298 K which is consistent with solvent loss from the sample. The peaks in the powder pattern still showed a reasonable match with a simulation from the 200 K crystal

structure, however. Repeated measurements indicated the sample was undergoing a slow transformation inside the diffractometer to a new phase, which was obtained in pure form by annealing at 340 K for 30 mins. Once formed, this new phase was stable at room temperature for at least a period of hours. Hence, the spin-crossover-active phase of **3[BF₄]₂** is not isostructural with the crystalline solvate, although it is likely to retain the interdigitated layers found in the terpyridine embrace structure (Fig. 2).

Only single crystalline samples of **3[BF₄]₂·2MeNO₂**, that are grown over a period of days, exhibit this behavior. When precipitated more rapidly from this solvent system, the compound forms an amorphous low-spin powder that absorbs atmospheric moisture. The response of this material to heating varies; some samples remain low-spin, while in others it induces a partial, gradual spin-crossover with a similar $T_{1/2}$ to the annealed single crystals. This presumably reflects differing levels of crystallinity between the samples. The perchlorate salt **3[ClO₄]₂** is similarly isolated from MeNO₂/Et₂O as an amorphous low-spin hydrate material, which sometimes contains a small spin-crossover fraction ($T_{1/2} \approx 330$ K, ≤ 15 % of the sample). Crystals of **3[ClO₄]₂·xMeNO₂** were obtained on one occasion, which suffered from twinning. However a preliminary structure solution showed they are not isostructural with **3[BF₄]₂·2MeNO₂**, but adopt an alternative version of the terpyridine embrace lattice.³² Compared to the **3[BF₄]₂·2MeNO₂** structure, the perchlorate crystal has a larger distance between the cation layers, which results in more anion and solvent disorder including some apparent void space in the lattice. Such an expansion of the space between the layers, leading to anion and solvent disorder, may explain the tendency of both salts to form amorphous hydrate material when rapidly precipitated from MeNO₂/Et₂O mixtures.

In an attempt to obtain solvent-free $3[\text{BF}_4]_2$ and $3[\text{ClO}_4]_2$ in crystalline form, these salts were synthesized in, or recrystallized from, a variety of other solvent/antisolvent combinations. Layering an acetone solution of hydrated metal salt with a chloroform solution of 2-bip yielded single crystals, which were found to be the chloroform solvates $3[\text{BF}_4]_2 \cdot y\text{CHCl}_3$ ($y \approx 1$) and $3[\text{ClO}_4]_2 \cdot \text{CHCl}_3$. Interestingly, these are not isostructural. The BF_4^- solvate ($C2/c$, $Z = 12$) suffered from extensive anion and solvent disorder (the solvent was treated using *SQUEEZE*²¹), but a refinement at 120 K demonstrated the main features of the structure. The asymmetric unit contains two crystallographically unique iron sites: a whole molecule, which is high-spin from its metric parameters; and a low-spin, C_2 -symmetric half-molecule (Table 2). In contrast, the asymmetric unit of $3[\text{ClO}_4]_2 \cdot \text{CHCl}_3$ ($P\bar{1}$, $Z = 2$) at 120 K contains just one iron site, which has an approximately 1:1 high-spin:low-spin state population which is resolved through disorder in one of the 2-bip ligands. A structure analysis of $3[\text{ClO}_4]_2 \cdot \text{CHCl}_3$ at 340 K was also achieved, where the ligand disorder is no longer apparent and the compound is fully high-spin (Table 2).

The high-spin $[\text{Fe}(2\text{-bip})_2]^{2+}$ centers in $3[\text{BF}_4]_2 \cdot y\text{CHCl}_3$ form three face-to-face $\pi \dots \pi$ interactions with two high-spin and one low-spin nearest neighbors, while each low-spin molecule participates in $\pi \dots \pi$ contacts with just two, high-spin cations (Fig. 4). This open pattern of inter-cation interactions leads to interdigitation of adjacent groups of π -stacked cations, affording a 3D network of $\pi \dots \pi$ interactions. In $3[\text{ClO}_4]_2 \cdot \text{CHCl}_3$, each $[\text{Fe}(2\text{-bip})_2]^{2+}$ molecule forms $\pi \dots \pi$ interactions to three neighbor cations, with a similar disposition to the high-spin cation in the BF_4^- structure. The fourth indazolyl donor, that does not participate in a $\pi \dots \pi$ interaction, is the one that exhibits the resolvable high- and low-spin disorder sites. The complex molecules in $3[\text{ClO}_4]_2 \cdot \text{CHCl}_3$ pack into discrete layers separated by anions and solvent,

although the local symmetry within the layers is too low for it to be considered an embrace-type structure (Fig. 5).¹⁵

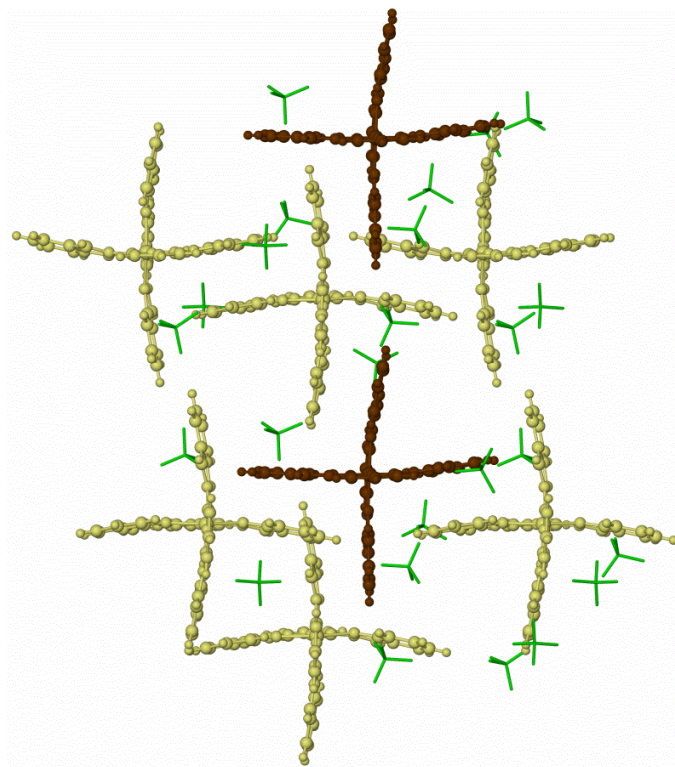


Figure 4. Packing diagram of $3[\text{BF}_4]_2 \cdot y\text{CHCl}_3$ at 120 K, showing the crystallographically distinct high-spin (yellow) and low-spin (brown) complex cations. The anions are de-emphasized for clarity, and the view is parallel to the [001] crystal vector. The color scheme is different from Figs. 2 and 5 because this is not a layered structure; the molecules in the top-right and bottom-left of the Figure are offset along c , and exhibit weak or negligible $\pi \dots \pi$ overlap with their nearest neighbor in the view.

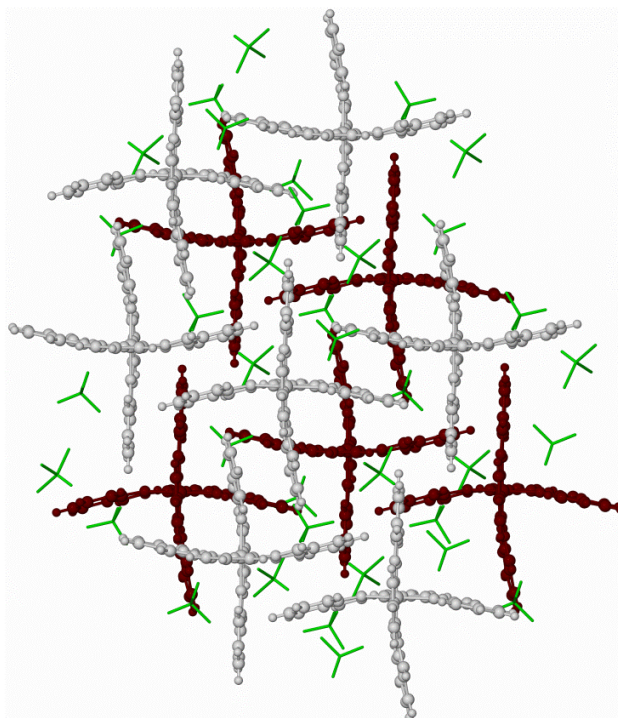


Figure 5. Packing diagram of $3[\text{ClO}_4]_2 \cdot \text{CHCl}_3$ at 120 K, viewed parallel to the $[110]$ crystal vector. The anions and solvent are de-emphasized for clarity. The cations, which are all crystallographically equivalent, pack into discrete layers; alternate layers in the Figure have the same color scheme as in Fig. 2.

Both the chloroform solvates retain their solvent on exposure to air, and lose it only sluggishly on heating by TGA. Loss of one equiv CHCl_3 from $3[\text{BF}_4]_2 \cdot \text{CHCl}_3$ was achieved near 480 K, while only 1 % mass loss was observed from $3[\text{ClO}_4]_2 \cdot \text{CHCl}_3$ at 393 K, the highest temperature studied on safety grounds. Magnetic susceptibility data show that $3[\text{BF}_4]_2 \cdot \text{CHCl}_3$ is high-spin at room temperature but undergoes a well-defined spin-crossover near 150 K in around one-third of its iron centers (Fig. 6). That is consistent with the 2:1 high:low spin state population in the crystallographic analysis of this compound at 120 K. Solid $3[\text{ClO}_4]_2 \cdot \text{CHCl}_3$ is essentially high-

spin at 350 K but undergoes a slow decrease in $\chi_M T$ on cooling to 180 K, where a more rapid spin-transition in *ca.* 50 % of the iron centres occurs with $T_{1/2} \approx 140$ K (Fig. 6). The $\chi_M T$ values at 120 K and 340 K (1.6 and 3.1 $\text{cm}^3 \text{mol}^{-1} \text{K}$, respectively) imply the sample is *ca.* 50 % and >90 % high-spin at those temperatures, in agreement with the crystal structures. The susceptibility curves from both compounds were unchanged after heating to 350 K, in agreement with their TGA data. No thermal hysteresis was observed in either of the chloroform solvate spin transitions, which confirms that the hysteretic behavior of annealed $3[\text{BF}_4]_2 \cdot 2\text{MeNO}_2$ (Fig. 3) is not an inherent property of the complex, and can be attributed to the terpyridine embrace lattice structure adopted by that crystal phase.

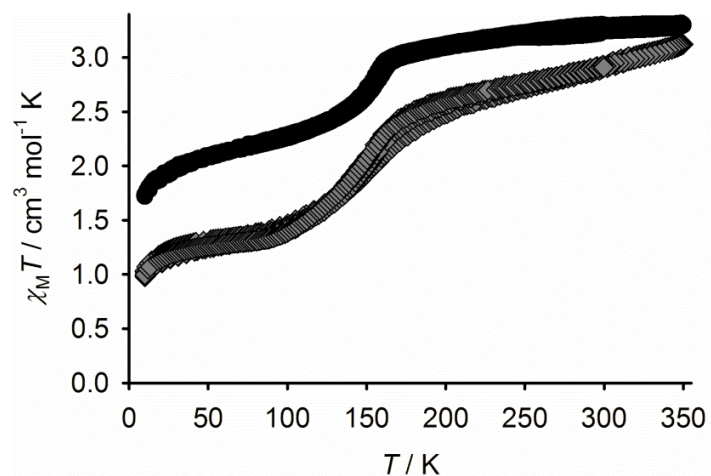


Figure 6. Magnetic susceptibility data for $3[\text{BF}_4]_2 \cdot y\text{CHCl}_3$ (●) and $3[\text{ClO}_4]_2 \cdot \text{CHCl}_3$ (◆). Both samples were run on a 298 → 3 → 350 → 3 → 298 K temperature ramp.

Single crystals of **4**[BF₄]₂·MeNO₂ and **4**[ClO₄]₂·MeNO₂ are isostructural, and contain the expected six-coordinate cation which is low-spin at 120 K (Fig. 7). Bulk samples of both salts are also low-spin in the solid state at room temperature. This can be attributed to a short intra-ligand steric contact between the pyridyl *H3* and indazolyl *H7* atoms, which are only 2.1 Å apart in the structure refinements (Fig. 7). These H...H contacts are oriented to disfavor the lengthening of the Fe–N bonds, that is a pre-requisite for spin-crossover. The same steric consideration also imposes a low-spin configuration onto **1**X₂ and **2**X₂ (X[−] = BF₄[−] and ClO₄[−]).²⁵ The crystal packing in **4**[BF₄]₂·MeNO₂ and **4**[ClO₄]₂·MeNO₂ is not of the embrace type,¹⁴ and neighboring complex molecules in the lattice only interact through weak van der Waals contacts. Variable temperature magnetic susceptibility data showed that dried samples of **4**[BF₄]₂ and **4**[ClO₄]₂ are also low-spin, between 5–300 K.

In contrast to the other complex salts in this work, **5**[BF₄]₂ and **5**[ClO₄]₂ could not be crystallized from organic solvents and were only obtained as solids following evaporation of their solutions to dryness. The resultant powders were analytically pure, but essentially amorphous by X-ray powder diffraction. Both compounds are predominantly high-spin at room temperature ($\chi_{\text{M}}T = 3.0 \text{ cm}^3\text{mol}^{-1}\text{K}$) and exhibit poorly defined, gradual and incomplete spin-state equilibria upon cooling which are consistent with their amorphous nature (Fig. S19, Supporting Information).

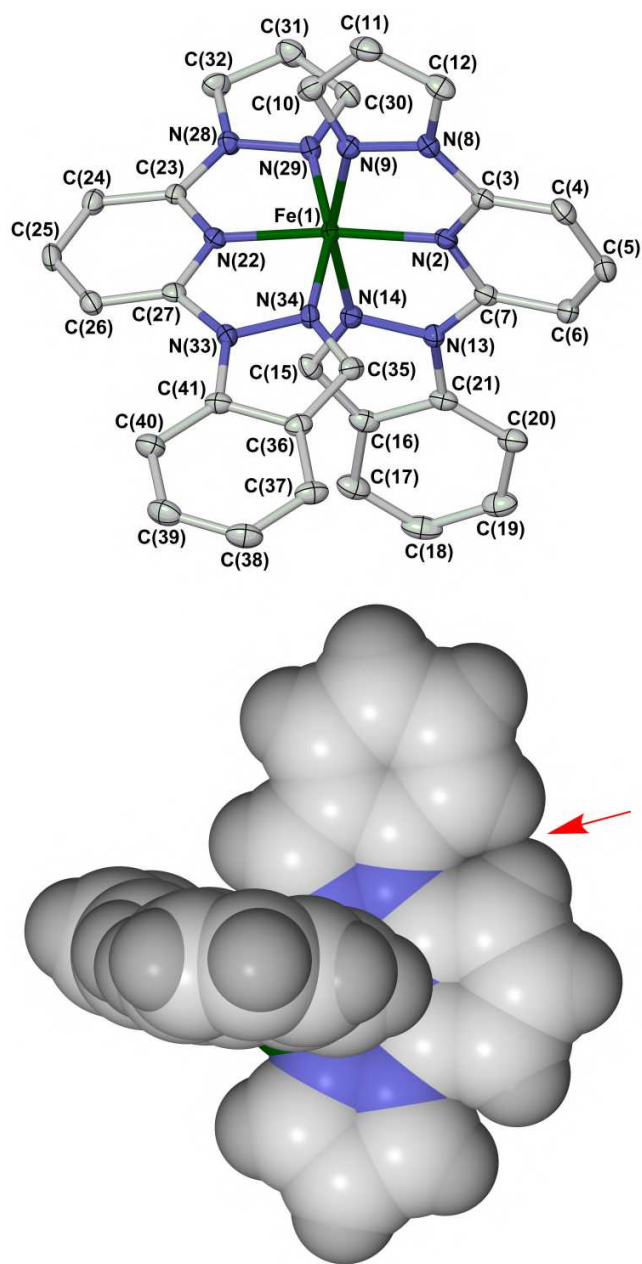


Figure 7. Top: view of the $[\text{Fe}(\text{1-ipp})_2]^{2+}$ dication in the structure of $4[\text{BF}_4]_2 \cdot \text{MeNO}_2$. Displacement ellipsoids are drawn at the 50 % probability level, and H atoms have been omitted. Bottom: space-filling view of $[\text{Fe}(\text{1-ipp})_2]^{2+}$, highlighting the intra-ligand H...H contact that imposes a low-spin state onto the iron center. Color code: C, white; N, blue; Fe, green.

Table 3 Selected bond lengths and angular parameters in **4[BF₄]₂·MeNO₂** and **4[ClO₄]₂·MeNO₂** (Å, deg). The atom numbering Scheme is shown in Fig. 7. Other details as in Table 2.

	4[BF₄]₂·MeNO₂	4[ClO₄]₂·MeNO₂
Fe(1)–N(2)	1.907(2)	1.8963(17)
Fe(1)–N(9)	1.967(3)	1.9710(18)
Fe(1)–N(14)	1.949(3)	1.9408(17)
Fe(1)–N(22)	1.898(2)	1.8928(17)
Fe(1)–N(29)	1.984(3)	1.9835(18)
Fe(1)–N(34)	1.957(3)	1.9582(18)
α	80.3(2)	80.40(14)
Σ	85.1(3)	84.2(2)
\varnothing	275	273
ϕ	173.18(10)	173.89(7)
θ	84.65(2)	84.77(2)

Solutions of [Fe(1-bip)₂]²⁺ are diamagnetic and low-spin by ¹H NMR,¹⁵ while the ¹H NMR spectra of **2[ClO₄]₂** and **4[ClO₄]₂** are only slightly contact shifted, implying they contain a small high-spin fraction at room temperature. That was confirmed by Evans method measurements in CD₃NO₂, which showed that they each exhibit $\chi_M T = 0.3 \text{ cm}^3 \text{ mol}^{-1} \text{ K}$ at 293 K, corresponding to a 1:9 high:low-spin population. Both compounds undergo thermal spin-transitions on warming, with $T_{1/2} = 343(2) \text{ K}$ (**2[ClO₄]₂**) and $350(2) \text{ K}$ (**4[ClO₄]₂**; Fig. 8).³³ In contrast, **3[ClO₄]₂** and **5[ClO₄]₂** are fully high-spin in solution at room temperature. Solutions of **3[ClO₄]₂** in CD₃CN remain high-spin within experimental error on cooling to 234 K, the lowest temperature accessible in that solvent; experiments in lower melting solvents were precluded on solubility grounds. The greater solubility of **5[ClO₄]₂** allowed it to be measured in (CD₃)₂CO, which

revealed a thermal spin-crossover with $T_{1/2} = 222(1)$ K (Fig. 8).³³ That is 26 K lower than for $[\text{Fe}(\text{1-bpp})_2]^{2+}$ in the same solvent.²⁶ The small stabilization of the complexes' high-spin state upon sequential replacement of pyrazol-1-yl by indazol-2-yl donors is consistent with the slightly lower basicity of the indazolyl groups (for example, the basic pK_{a} s of 1-methylpyrazole and 2-methylindazole are 2.06 and 2.01, respectively³⁴). In contrast, the similar $T_{1/2}$ values of $\mathbf{2}[\text{ClO}_4]_2$ and $\mathbf{4}[\text{ClO}_4]_2$ support the suggestion that the most important factor in the spin-states of the 1-indazolyl ligand complexes is their sterically imposed conformational rigidity (Fig. 7).²⁵

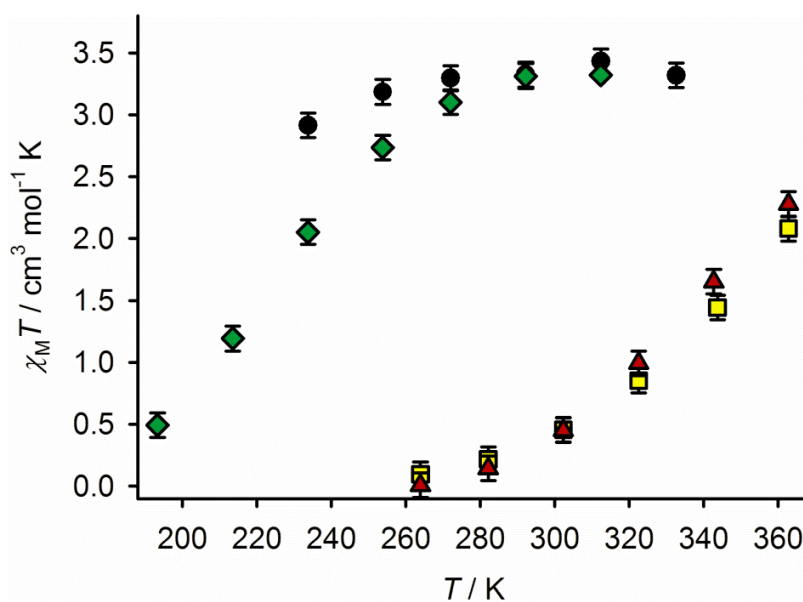


Figure 8. Solution-phase magnetic susceptibility data for: $\mathbf{2}[\text{ClO}_4]_2$ in CD_3NO_2 (red triangles); $\mathbf{3}[\text{ClO}_4]_2$ in CD_3CN (black circles); $\mathbf{4}[\text{ClO}_4]_2$ in CD_3NO_2 (yellow squares); and $\mathbf{5}[\text{ClO}_4]_2$ in $(\text{CD}_3)_2\text{CO}$ (green diamonds).³³

The spin-states of the complexes in solution at room temperature are supported by UV/vis spectroscopy in MeCN, in that the low-spin compounds **1**[ClO₄]₂, **2**[ClO₄]₂ and **4**[ClO₄]₂ exhibit an envelope of MLCT absorptions centred around $\lambda_{\text{max}} = 420 \text{ nm}$ ($\epsilon_{\text{max}} = 4\text{-}6 \times 10^3 \text{ dm}^3 \text{ mol}^{-1} \text{ cm}$), that is not resolved for high-spin **3**[ClO₄]₂ and **5**[ClO₄]₂ (Fig. 9). However, a strong $\pi \rightarrow \pi^*$ band near 325 nm is more intense in the high-spin complexes than in the low-spin ones, reflecting the stronger absorptions exhibited by indazol-2-yl substituents in this region compared to indazol-1-yl groups.³⁵ Since this ligand-based absorption tails into the visible region, the colors of the high-spin and low-spin complexes in this work are all a similar orange-brown.

The different isomers of the bip and ipp ligands all exhibit blue fluorescence in chloroform solution at room temperature (Fig. 9). The fluorescence spectra of 1,2-bip and 2-bip are similar, with vibrationally structured emissions of comparable intensity in the near-UV ($\lambda_{\text{max}}^{\text{em}} = 375 \text{ nm}$). Emission from 1-bip under the same conditions is slightly blue-shifted, showing $\lambda_{\text{max}}^{\text{em}} = 355 \text{ nm}$ with additional low- and high-wavelength shoulders. These profiles closely resemble the emission spectra of 2-methylindazole and 1-methylindazole, respectively, and hence are clearly indazole-centred.^{35,36} The emissions from 1-ipp and 2-ipp are much weaker and less structured than for the *bis*-indazolyl ligands but exhibit the same trend, with emission from 1-ipp ($\lambda_{\text{max}}^{\text{em}} = 347 \text{ nm}$) lying at lower wavelength than for 2-ipp ($\lambda_{\text{max}}^{\text{em}} = 392 \text{ nm}$).

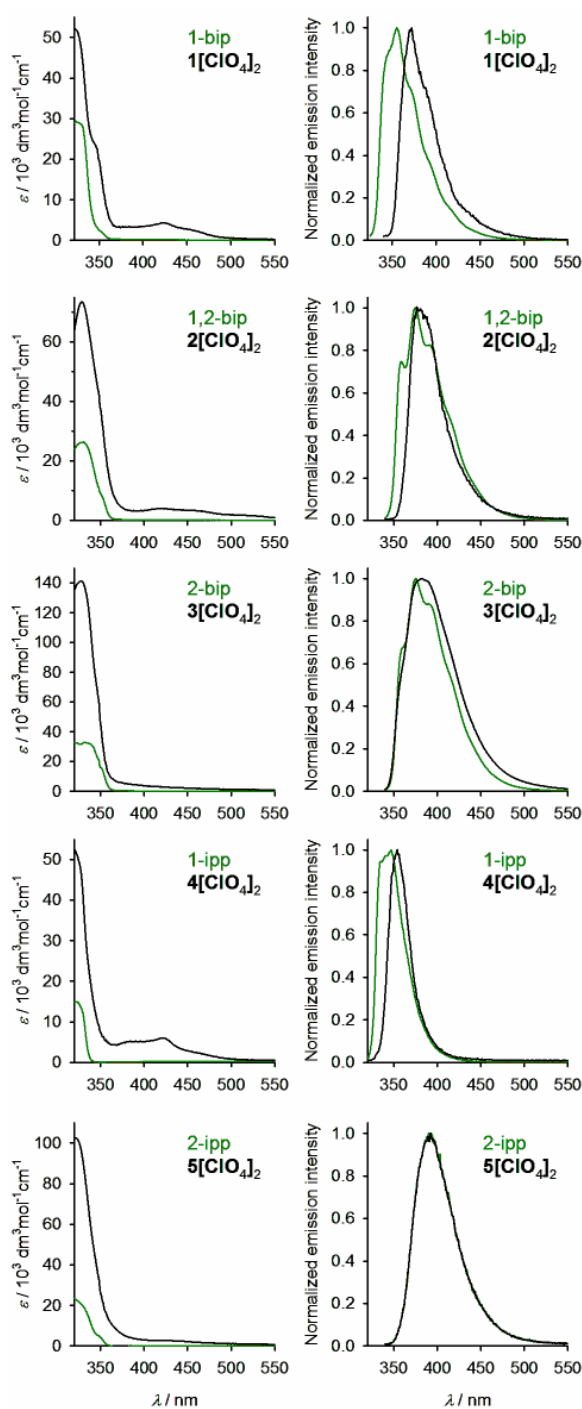


Figure 9. Left: absorption spectra, and right: normalized emissions from the free ligands in CHCl_3 (green) and the corresponding iron(II) complexes in MeCN (black). These data, and the fluorescence excitation wavelengths, are listed in the Supporting Information (Tables S6 and S7).

The fluorescence of the complexes was measured in MeCN, for solubility reasons (Fig. 9). Notably **3**[ClO₄]₂ and **5**[ClO₄]₂, which are high-spin in solution at room temperature, are strong emitters despite their paramagnetism. Although it has less vibrational structure, the fluorescence profile from **3**[ClO₄]₂ ($\lambda_{\text{max}}^{\text{em}} = 383$ nm) is otherwise very similar to the corresponding free ligand 2-bip. The normalized emission profiles of 2-ipp and **5**[ClO₄]₂ ($\lambda_{\text{max}}^{\text{em}} = 392$ nm) are likewise superimposable, which probably reflects the absence of vibrational structure on that weak free ligand emission. In contrast **1**[ClO₄]₂ ($\lambda_{\text{max}}^{\text{em}} = 372$ nm) and **4**[ClO₄]₂ ($\lambda_{\text{max}}^{\text{em}} = 354$ nm), which are ≥ 90 % low-spin at room temperature, both exhibit slightly red-shifted emissions compared to their free ligands. The fluorescence of low-spin **2**[ClO₄]₂, which contains both indazol-1-yl and indazol-2-yl functions, is a combination of these two behaviors; its emission profile has an almost identical maximum to the parent 1,2-bip ligand ($\lambda_{\text{max}}^{\text{em}} = 377$ nm), but is significantly narrower at lower wavelengths (Fig. 9). Notably the shifts in all these ligand-based emission envelopes upon complexation to iron, resemble the effects of protonation of 1-methylindazole (suppression of low-wavelength emission components and enhancement of higher wavelength bands) or 2-methylindazole (a small red-shifting of the emission maximum, with no other change in the band shape).³⁶ Although they should be interpreted with care since they were measured under aerobic conditions, the relative fluorescence intensities for the complexes follow the order **3**[ClO₄]₂ > **4**[ClO₄]₂ \approx **5**[ClO₄]₂ > **1**[ClO₄]₂ \approx **2**[ClO₄]₂. Hence, no conclusion about the ability of the high- or low-spin states of the complexes to quench the ligand emission could be drawn from this preliminary study.

Discussion

One important contribution from this work relates to structure:function relationships in molecular spin-crossover materials. The solvate $3[\text{BF}_4]_2 \cdot 2\text{MeNO}_2$ crystallizes in the terpyridine embrace lattice motif that is adopted by several $[\text{Fe}(1\text{-bpp})_2]^{2+}$ derivatives, including $[\text{Fe}(1\text{-bpp})_2][\text{BF}_4]_2$ itself.¹¹⁻¹⁴ After desolvation of these crystals, $3[\text{BF}_4]_2$ exhibits spin-crossover with an almost identical midpoint temperature to $[\text{Fe}(1\text{-bpp})_2][\text{BF}_4]_2$, but with a hysteresis loop that is widened from 3 K to 16-20 K. Both these crystalline compounds exhibit closely interdigitated cations, with no other intermolecular interactions to complicate their structure:function relationships. We therefore conclude that the increased hysteresis in $3[\text{BF}_4]_2$ is caused by the extended face-to-face contact between the annelated arms of $[\text{Fe}(2\text{-bip})_2]^{2+}$. That is a useful confirmation of our previously proposed magnetostructural correlation in spin-crossover terpyridine embrace crystals.¹² Notably two other solvate salts of $[\text{Fe}(2\text{-bip})_2]^{2+}$ that adopt different modes of crystal packing, $3[\text{BF}_4]_2 \cdot y\text{CHCl}_3$ and $3[\text{ClO}_4]_2 \cdot \text{CHCl}_3$, exhibit more gradual and incomplete spin-transitions without thermal hysteresis. Hence the transition cooperativity in desolvated $3[\text{BF}_4]_2 \cdot 2\text{MeNO}_2$ appears to be specific to the terpyridine embrace lattice type.

A related literature system is $[\text{Fe}(\text{bzimpy})_2][\text{ClO}_4]_2 \cdot \text{H}_2\text{O}$ (bzimpy = 2,6-*bis*{benzimidazol-2-yl}pyridine), which also adopts a terpyridine embrace structure and exhibits a spin-transition that occurs at higher temperature than for $3[\text{BF}_4]_2$, but is otherwise very comparable ($T_{1/2} = 403$ K, $\Delta T = 12$ K).³⁷ Although this requires further investigation, terpyridine embrace lattices with iron(II) complexes of annelated *tris*-imine ligands like 2-bip and bzimpy might consistently exhibit hysteresis that is 10-15 K wider than their non-annelated analogues. Also worth comment are complexes of the $[\text{Fe}(3\text{-bpp})_2]^{2+}$ type (3-bpp = 2,6-di{1*H*-pyrazol-3-yl}pyridine, an isomer of 1-bpp),³⁸ which are stereochemically similar to $[\text{Fe}(1\text{-bpp})_2]^{2+}$ and sometimes adopt terpyridine embrace structures which can exhibit hysteretic spin-transitions.^{30,39} However, the chemistry of

$[\text{Fe}(\text{3-bpp})_2]^{2+}$ derivatives is complicated by hydrogen bonding to its ligand N–H groups, which strongly influences the spin state of the iron centre.²⁸ Hence the $[\text{Fe}(\text{1-bpp})_2]^{2+}/[\text{Fe}(\text{2-bip})_2]^{2+}$ system, which lacks this feature, is a more reliable testbed to rationally deconvolute the structure: function relationships in this type of compound.

The ligand-based blue emission exhibited by the indazolyl ligands in this work in solution, under ambient conditions, is retained upon complexation to iron. The indazol-1-yl ligand complexes **1** $[\text{ClO}_4]_2$ and **4** $[\text{ClO}_4]_2$ exhibit a small red-shift in their emission maximum compared to the corresponding free ligands, whereas the emission maxima from the indazol-2-yl ligands and their complexes **3** $[\text{ClO}_4]_2$ and **5** $[\text{ClO}_4]_2$ are more similar (Fig. 9). It is tempting to attribute this different behavior to the spin states of **1** $[\text{ClO}_4]_2$ and **4** $[\text{ClO}_4]_2$ (low-spin) and **3** $[\text{ClO}_4]_2$ and **5** $[\text{ClO}_4]_2$ (high-spin) under the conditions of measurement. However, the similarity of these data to a literature study of the protonation of 1-methylindazole and 2-methylindazole, as monitored by fluorescence, is striking.³⁶ Therefore, the changes in emission wavelength upon coordination of the ligands in this work are more likely to be simply a consequence of complexing the indazolyl rings, with no obvious contribution from the iron spin state.

This observation has consequences for the design of fluorescent spin-crossover compounds, which have been pursued by several groups with mixed success.⁴⁰⁻⁴⁶ The strongest coupling between spin-crossover and emission has been achieved using remote fluorophores tethered to iron complex centers, either in individual molecules^{40,41} or more complex nanostructures.^{42,43} This antenna effect may be a more promising approach towards multifunctional fluorescent switches, than compounds where the emissive group is directly ligated to the iron center as in this work.

Conclusions

A new synthetic protocol, employing milder reaction conditions than in earlier reports,^{15,16} has allowed all the isomers of 2,6-di(indazolyl)pyridine (bip) and 2-(indazolyl)-6-(pyrazolyl)pyridine (ipp) to be isolated for the first time. These are annelated analogues of the well-known ligand 2,6-bis{pyrazol-1-yl}pyridine, whose iron(II) complex is an important spin-crossover compound.¹¹ All the complexes of ligands with indazol-1-yl donor groups (**1X₂**, **2X₂** and **4X₂**; X⁻ = BF₄⁻ or ClO₄⁻; Chart 1) are low-spin in the solid state below 300 K, in agreement with previous work, and are also fully or predominantly low-spin in solution at room temperature. This is attributed to conformational rigidity of the ligands, enforced by an intra-ligand steric contact between indazol-1-yl and pyridyl C–H groups (Fig. 7).²⁵ In contrast, complexes of the indazol-2-yl ligands, **3X₂** and **5X₂**, are high-spin at room temperature. Solution phase data show that, in the absence of steric clashes or crystal packing effects, increasing the number of indazol-2-yl donors in the tridentate ligands progressively stabilizes the high-spin state of the complexes. All the compounds exhibit a blue ligand-centered emission, which does not obviously correlate with the spin states of the complexes.

ASSOCIATED CONTENT

Supporting Information. Additional crystallographic data, Figures and Tables; TGA, magnetic susceptibility, UV/vis and fluorescence data; and, crystallographic information files (CIF). This material is available free of charge via the Internet at <http://pubs.acs.org>. CCDC 999073 and 999074 (**3[BF₄]₂·2MeNO₂**), 1026356 (1-bip), 1026357 (1,2-bip), 1026358 (2-bip),

1026359 (**3**[BF₄]₂·yCHCl₃), 1026360 and 1026361 (**3**[ClO₄]₂·CHCl₃), 1026362-1026364 (2-fluoro-6-(indazol-2-yl)pyridine), 1026365 (**4**[BF₄]₂·MeNO₂), 1026366 (2-ipp) and 1026367 (**4**[ClO₄]₂·MeNO₂) contain the supplementary crystallographic data for this Paper. These data can be obtained free of charge from the Cambridge Crystallographic Data Center via www.ccdc.cam.ac.uk/data_request/cif.

AUTHOR INFORMATION

Corresponding Author

*Email: m.a.halcrow@leeds.ac.uk

Notes

The authors declare no competing financial interest.

ACKNOWLEDGMENT

This work was funded by the EPSRC (EP/I014039/1, EP/K012568/1 and EP/K00512X/1).

REFERENCES

- (1) Gütlich, P.; Goodwin, H. A. (eds.) *Spin Crossover in Transition Metal Compounds I–III, Topics in Current Chemistry*; Springer-Verlag: Berlin, 2004; Vols. 233–235.
- (2) Halcrow, M. A. (ed), *Spin-crossover materials - properties and applications*, John Wiley & Sons, Ltd.: New York, 2013, p. 568.
- (3) (a) Gütlich, P. *Eur. J. Inorg. Chem.* **2013**, 581–591. (b) Gütlich, P.; Gaspar, A. B.; Garcia, Y. *Beilstein J. Org. Chem.* **2013**, 9, 342–391.
- (4) Bousseksou, A.; Molnár, G.; Salmon, L.; Nicolazzi, W. *Chem. Soc. Rev.* **2011**, 40, 3313–3335.
- (5) (a) Cavallini, M. *Phys. Chem. Chem. Phys.* 2012, **14**, 11867–11876. (b) Shepherd, H. J.; Molnár, G.; Nicolazzi, W.; Salmon, L.; Bousseksou, A. *Eur. J. Inorg. Chem.* **2013**, 653–661. (c) Molnár, G.; Salmon, L.; Nicolazzi, W.; Terki, F.; Bousseksou, A. *J. Mater. Chem. C* **2014**, 2, 1360–1366.
- (6) Shepherd, H. J.; Gural'skiy, I. A.; Quintero, C. M.; Tricard, S.; Salmon, L.; Molnár, G.; Bousseksou, A. *Nat. Commun.* **2013**, 4, 2607/1–2607/9.
- (7) Kröber, J.; Coddjovi, E.; Kahn, O.; Grolrière, F.; Jay, C. *J. Am. Chem. Soc.* **1993**, 115, 9810–9811.
- (8) Bonhommeau, S.; Molnár, G.; Galet, A.; Zwick, A.; Real, J. A.; McGarvey, J. J.; Bousseksou, A. *Angew. Chem. Int. Ed.* **2005**, 44, 4069–4073.
- (9) Schäfer, B.; Rajnák, C.; Šalitroš, I.; Fuhr, O.; Klar, D.; Schmitz-Antoniak, C.; Weschke, E.; Wende, H.; Ruben, M. *Chem. Commun.* **2013**, 49, 10986–10988.

- (10) Halcrow, M. A. *Chem. Soc. Rev.* **2011**, *40*, 4119–4142.
- (11) Halcrow, M. A. *Coord. Chem. Rev.* **2009**, *253*, 2493–2514.
- (12) Pritchard, R.; Kilner, C. A.; Halcrow, M. A. *Chem. Commun.* **2007**, 577–579.
- (13) (a) Carbonera, C.; Costa, J. S.; Money, V. A.; Elhaïk, J.; Howard, J. A. K.; Halcrow, M. A.; Létard, J.-F. *Dalton Trans.* **2006**, 3058–3066. (b) Pritchard, R.; Lazar, H.; Barrett, S. A.; Kilner, C. A.; Asthana, S.; Carbonera, C.; Létard, J.-F.; Halcrow, M. A. *Dalton Trans.* **2009**, 6656–6666. (c) Mohammed, R.; Chastanet, G.; Tuna, F.; Malkin, T. L.; Barrett, S. A.; Kilner, C. A.; Létard, J.-F.; Halcrow, M. A. *Eur. J. Inorg. Chem.* **2013**, 819–831.
- (14) (a) Scudder, M. L.; Goodwin, H. A.; Dance, I. G. *New J. Chem.* **1999**, *23*, 695–705. (b) McMurtrie, J.; Dance, I. *CrystEngComm* **2005**, *7*, 216–229. (c) McMurtrie, J.; Dance, I. *CrystEngComm* **2010**, *12*, 2700–2710.
- (15) Pritchard, R.; Kilner, C. A.; Halcrow, M. A. *Tetrahedron Lett.* **2009**, *50*, 2484–2486.
- (16) Duncan, N. C.; Garner, C. M. *Tetrahedron Lett.* **2011**, *52*, 5214–5216.
- (17) Starck, M.; Kadjane, P.; Bois, E.; Darbouret, B.; Incamps, A.; Ziessel, R.; Charbonnière, L. J. *Chem. Eur. J.* **2011**, *17*, 9164–9179.
- (18) Schmidt, A.; Beutler, A.; Snovydovych, B. *Eur. J. Org. Chem.* **2008**, 4073–4095.
- (19) Sheldrick, G. M. *Acta Cryst. Sect. A* **2008**, *64*, 112–122.
- (20) Barbour, L. J. *J. Supramol. Chem.* **2001**, *1*, 189–191.
- (21) Spek, A. L. *J. Appl. Cryst.* **2003**, *36*, 7–13.

- (22) O'Connor, C. J. *Prog. Inorg. Chem.* **1982**, *29*, 203–283.
- (23) (a) Evans, D. F. *J. Chem. Soc.* **1959**, 2003–2005. (b) Schubert, E. M. *J. Chem. Educ.* **1992**, *69*, 62.
- (24) (a) Philip, J. C.; Oakley, H. B. *J. Chem. Soc. Trans.* **1924**, *125*, 1189–1195. (b) Felsing, W. A.; Durban, S. A. *J. Am. Chem. Soc.* **1926**, *48*, 2885–2893. (c) García, B.; Ortega, J. C. *J. Chem. Eng. Data* **1988**, *33*, 200–204.
- (25) The salts $\mathbf{1X}_2$ and $\mathbf{2X}_2$ ($X^- = \text{BF}_4^-$ and ClO_4^-) are low-spin in the solid at room temperature (ref. 15 and Fig. S19). That probably reflects short contacts between the pyridyl *H3/H5* atoms and the indazol-1-yl *H7* atoms in the coordinated ligands, which inhibit the expansion of the metal coordination sphere that would accompany a transition to a high-spin state (Fig. S5). The same steric contacts also stabilize the low-spin state of $\mathbf{4}[\text{BF}_4]_2$ and $\mathbf{4}[\text{ClO}_4]_2$ (Fig. 7).
- (26) (a) McCusker, J. K.; Rheingold, A. L.; Hendrickson, D. N. *Inorg. Chem.* **1996**, *35*, 2100–2112. (b) Guionneau, P.; Marchivie, M.; Bravic, G.; Létard, J.-F.; Chasseau, D. *Top. Curr. Chem.* **2004**, *234*, 97–128.
- (27) Holland, J. M.; McAllister, J. A.; Kilner, C. A.; Thornton-Pett, M.; Bridgeman, A. J.; Halcrow, M. A. *J. Chem. Soc. Dalton Trans.* **2002**, 548–554.
- (28) Kershaw Cook, L. J.; Mohammed, R.; Sherborne, G.; Roberts, T. D.; Alvarez, S.; Halcrow, M.A. *Coord. Chem. Rev.*, doi: 10.1016/j.ccr.2014.08.006.

(29) Kröber, J.; Audière, J. P.; Claude, R.; Codjovi, E.; Kahn, O.; Haasnoot, J. G.; Grolière, F.; Jay, C.; Bousseksou, A.; Linares, J.; Varret, F.; Gonthier-Vassal, A. *Chem. Mater.* **1994**, *6*, 1404–1412.

(30) Roberts, T. D.; Tuna, F.; Malkin, T. L.; Kilner, C. A.; Halcrow, M. A. *Chem. Sci.* **2012**, *3*, 349–354.

(31) Sorai, M.; Nakazawa, Y.; Nakano, M.; Miyazaki, Y. *Chem. Rev.* **2013**, *113*, PR41–PR122.

(32) A preliminary solution was obtained from a twinned crystal of formula $3[\text{ClO}_4]_2 \cdot x\text{MeNO}_2$ ($x \approx 1$): $\text{C}_{39}\text{H}_{29}\text{Cl}_2\text{FeN}_{11}\text{O}_{10}$, M_r 938.48, monoclinic, $P2_1/c$, $a = 10.0115(3)$, $b = 26.3734(9)$, $c = 19.4545(5)$ Å, $\beta = 90.439(3)^\circ$, $V = 5136.6(3)$ Å³, $Z = 4$, $D_{\text{calc}} = 1.210$ gcm⁻³, $T = 100(2)$ K, 16488 measured reflections, 8975 independent reflections, $R_{\text{int}} = 0.046$, $R_1 [I > 2\sigma(I)] = 0.190$, wR_2 [all data] = 0.499. A packing diagram for this structure is shown in Fig. S11.

(33) The use of different NMR solvents to measure these compounds was dictated by their solubilities, and the requirement for solvents with appropriate liquid ranges for their different spin-transitions. The weakly interacting solvents used in this work will have a negligible effect on the measured spin state properties of the complexes. See *e.g.* Barrett, S. A.; Kilner, C. A.; Halcrow, M. A. *Dalton Trans.* **2011**, *40*, 12021–12024.

(34) Catalan, J.; Abboud, J. L. M.; Elguero, J. *Adv. Heterocycl. Chem.* **1987**, *41*, 187–274.

(35) Noda, M.; Hirota, N.; Sumitani, M.; Yoshihara, K. *J. Phys. Chem.* **1985**, *89*, 399–401.

(36) Catalán, J.; del Valle, J. C.; Claramunt, R. M.; Boyer, G.; Laynez, J.; Gómez, J.; Jiménez, P.; Tomás, F.; Elguero, J. *J. Phys. Chem.* **1994**, *98*, 10606–10612.

- (37) Boča, R.; Boča, M.; Dlháň, L.; Falk, K.; Fuess, H.; Haase, W.; Jaroščiak, R.; Papánková, B.; Renz, F.; Vrbová, M.; Werner, R. *Inorg. Chem.* **2001**, *40*, 3025–3033.
- (38) Craig, G. A.; Roubeau, O.; Aromí, G. *Coord. Chem. Rev.* **2014**, *269*, 13–31.
- (39) (a) Sugiyarto, K. H.; Scudder, M. L.; Craig, D. C.; Goodwin, H. A. *Aust. J. Chem.* **2000**, *53*, 755–765. (b) Craig, G. A.; Costa, J. S.; Roubeau, O.; Teat, S. J.; Aromí, G. *Chem. Eur. J.* **2011**, *17*, 3120–3127.
- (40) Garcia, Y.; Robert, F.; Naik, A. D.; Zhou, G.; Tinant, B.; Robeyns, K.; Michotte, S.; Piraux, L. *J. Am. Chem. Soc.* **2011**, *133*, 15850–15853.
- (41) (a) Piguet, C.; Rivara-Minten, E.; Bernardinelli, G.; Bünzli, J.-C. G.; Hopfgartner, G. *J. Chem. Soc. Dalton Trans.* **1997**, 421–433; (b) Edder, C.; Piguet, C.; Bünzli, J.-C. G.; Hopfgartner, G. *Chem. Eur. J.* **2001**, *7*, 3014–3024.
- (42) Matsuda, M.; Isozaki, H.; Tajima, H. *Chem. Lett.* **2008**, *37*, 374–375.
- (43) (a) Salmon, L.; Molnár, G.; Zitouni, D.; Quintero, C.; Bergaud, C.; Micheau, J.-C.; Bousseksou, A. *J. Mater. Chem.* **2010**, *20*, 5499–5503. (b) Titos-Padilla, S.; Herrera, J. M.; Chen, X.-W.; Delgado, J. J.; Colacio, E. *Angew. Chem. Int. Ed.* **2011**, *50*, 3290–3293. (c) Wang, C.-F.; Li, R.-F.; Chen, X.-Y.; Wei, R.-J.; Zheng, L.-S.; Tao, J. *Angew. Chem. Int. Ed.*, doi: 10.1002/anie.201410454.
- (44) Hasegawa, M.; Renz, F.; Hara, T.; Kikuchi, Y.; Fukuda, Y.; Okubo, J.; Hoshi, T.; Linert, W. *Chem. Phys.* **2002**, *277*, 21–30.
- (45) (a) Tovee, C. A.; Kilner, C. A.; Thomas, J. A.; Halcrow, M. A. *CrystEngComm* **2009**, *11*, 2069–2077. (b) Kershaw Cook, L. J.; Halcrow, M. A. *Polyhedron* **2015**, *87*, 91–97.

(46) González-Prieto, R.; Fleury, B.; Schramm, F.; Zoppellaro, G.; Chandrasekar, R.; Fuhr, O.; Lebedkin, S.; Kappes, M.; Ruben, M. *Dalton Trans.* **2011**, 40, 7564–7570.

SYNOPSIS

All the isomers of 2,6-di(indazolyl)pyridine (bip) and 2-(indazolyl)-6-(pyrazol-1-yl)pyridine (ipp) have been isolated, and their iron(II) complexes prepared. Annealed crystals of $[\text{Fe}(\text{2-bip})_2][\text{BF}_4]_2 \cdot 2\text{MeNO}_2$ exhibit a cooperative spin-transition near room temperature, with a 16 K thermal hysteresis loop. All the ligands and complexes exhibit indazolyl-based fluorescence in solution at room temperature. The emission profile of the complexes changes according to which indazolyl isomer is present, but is apparently independent of the iron spin state.

